Materials Transactions, Vol. 42, No. 2 (2001) pp. 372 to 375

RAPID PUBLICATION

Nanocrystalline Icosahedral Phase Formation in Melt Spun Ti–Zr–Ni Alloys

B. S. Murty[1,*], W. T. Kim[2], D. H. Kim[3] and K. Hono[1]

[1]*National Research Institute for Metals, Tsukuba 305-0047, Japan*
[2]*Department of Physics, Chongju University, Chongju 360-764, Korea*
[3]*Department of Metallurgical Engineering, Yonsei University, Seoul 120-749, Korea*

The paper reports Icosahedral phase (i-phase) formation in the nanocrystalline state in $Ti_{55}Zr_{20}Ni_{25}$ and $Zr_{55}Ti_{25}Ni_{20}$ alloys. While nanocrystalline i-phase forms directly from the melt during melt spinning at low wheel velocity of 20 m/s, nanoquasicrystallization of amorphous phase has been observed on subsequent annealing after melt spinning at higher wheel velocities of 30 and 40 m/s. The i-phase is stable up to 873 K in Ti-rich alloy, while it transforms to crystalline phases in Zr-rich alloy below this temperature. The i-phase formed both directly from the melt and from the amorphous phase is much finer in Zr-rich alloy compared to Ti-rich alloy.

(Received October 26, 2000; Accepted December 26, 2000)

Keywords: *metallic glass, quasicrystal, melt spinning, phase transformations, transmission electron microscopy (TEM)*

1. Introduction

Since the early report by Köster *et al.*,[1] a number of investigators have reported[2–7] nanoquasicrystallization of Zr-based amorphous alloys. All these reports deal with the formation of icosahedral phase (i-phase) as a transient metastable phase during the crystallization of the metallic glass. While the early investigators felt the necessity of a multicomponent alloy for the i-phase formation, the present authors have shown that it can form even in binary Zr–Pd alloys.[7] In a major breakthrough, very recently i-phase formation is observed directly by melt spinning in Zr–Pt[8,9] and Zr–Ni–Mn[10] alloys. Li *et al.*[10] reported that Mn is essential for i-phase formation in Zr–Ni–Mn alloy. Though i-phase formation in the melt spun Zr alloys is new, it is an established fact in Ti based alloys and a number of reports exist on its formation in rapidly solidified Ti–Zr–Ni alloys.[11–13] In fact, metastable i-phase has been found in a wide composition range,[11] while stable i-phase forms in a narrow composition range.[13] However, i-phase reported in the Ti–Zr–Ni alloys is coarse grained (>200 nm). I-phase in general is known to be brittle, while the formation of nanocrystalline i-phase in the amorphous matrix appears to strengthen the Zr alloys without any significant loss of ductility.[4] Thus, the present work aimed at synthesizing the i-phase in the nanocrystalline state by controlled crystallization of the amorphous phase at two compositions ($Ti_{55}Zr_{20}Ni_{25}$ and $Zr_{55}Ti_{25}Ni_{20}$), which are close to the ternary eutectics in this system.[11] It is well known that amorphous phase is stabilized at the deep eutectic compositions, which justifies the choice of compositions for the present work.

2. Experimental Details

$Ti_{55}Zr_{20}Ni_{25}$ and $Zr_{55}Ti_{25}Ni_{20}$ alloys were prepared by arc melting of high purity metals (99.9%Zr and Ti, 99.99%Ni). The alloys were rapidly solidified by single roller melt spinning at wheel surface velocities of 20, 30 and 40 m/s in a reduced Ar atmosphere. X-ray diffraction (XRD) studies were carried out using Rigaku diffractometer (RINT 2500) with Cu K_α radiation. The thermal stability of the melt spun alloys was studied by differential scanning calorimetry (DSC) using Perkin-Elmer Pyris-1 at a heating rate of 40 K/min. Transmission electron microscopy (TEM) studies were carried out using a Philips CM200 microscope. The samples for TEM studies were prepared by ion milling.

3. Results and Discussion

Figures 1(a) and (b) are the XRD patterns of the melt spun $Ti_{55}Zr_{20}Ni_{25}$ and $Zr_{55}Ti_{25}Ni_{20}$ alloys, respectively, at different wheel velocities. The XRD patterns at 20 m/s for both the compositions could be indexed as i-phase based on the Elser's[14] indexing scheme. The quasilattice constant for the above two compositions is 0.5042 and 0.5274 nm, respectively. The higher quasilattice constant of Zr-rich alloy is expected from the larger atomic radius of Zr (0.159 nm) compared to Ti (0.145 nm). Amorphous phase forms in these alloys at melt spinning wheel velocities of 30 and 40 m/s (Figs. 1(a) and (b)). The TEM observation of these alloys melt spun at 20 m/s has shown single phase microstructure of i-phase, suggesting that both these alloys fall into the i-phase field in this system.[11] Figures 2(a) and (b) are the TEM bright field image and selected area electron diffraction/microdiffraction patterns (insets of Figs. 2(a) and (b), respectively) of melt spun $Ti_{55}Zr_{20}Ni_{25}$ and $Zr_{55}Ti_{25}Ni_{20}$ alloys, respectively, at 20 m/s. The i-phase grains in case of Zr-rich alloy are much finer (10–20 nm) than those in Ti-rich alloy (30–100 nm). The electron diffraction patterns (insets of Figs. 2(a) and (b)) confirm the quasicrystalline nature of these grains. It is interesting to note that though the grain size of i-phase is coarser in Ti-rich alloy, the XRD pattern of the alloy shows broader peaks compared to Zr-rich alloy (Figs. 1(a) and (b)), suggesting the possible presence of phason strains in the former.

Figure 3(a) shows the DSC traces of the Ti-rich alloy at different melt spun wheel velocities. At 20 m/s, the alloy has not shown any significant peaks in its DSC trace. The XRD pattern of this alloy isochronally annealed in DSC at 873 K

*On leave from Indian Institute of Technology, Kharagpur 721 302, India.

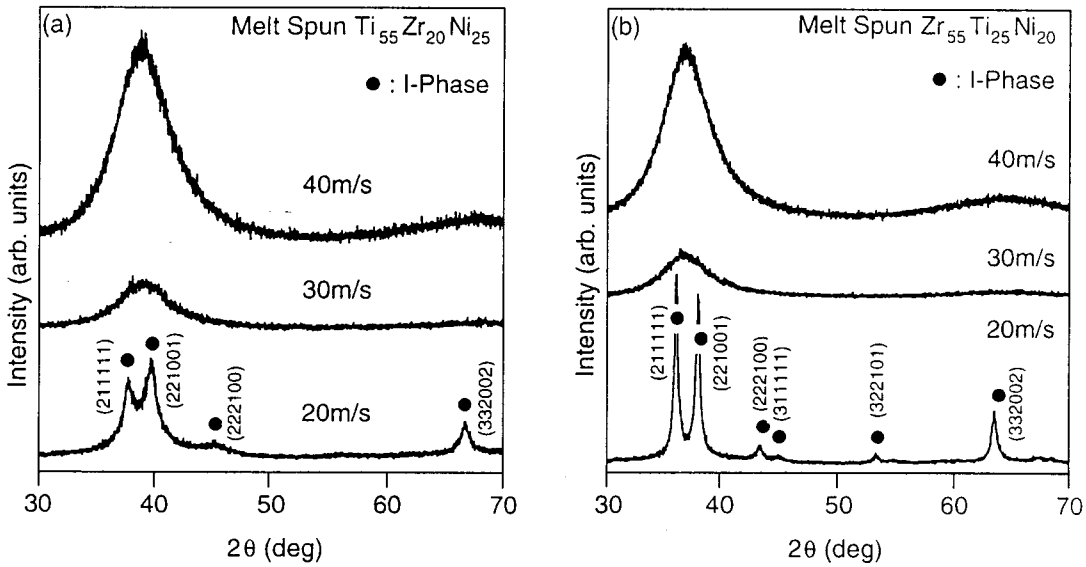

Fig. 1 XRD patterns of (a) $Ti_{55}Zr_{20}Ni_{25}$ and (b) $Zr_{55}Ti_{25}Ni_{20}$ alloys melt spun at 20, 30 and 40 m/s.

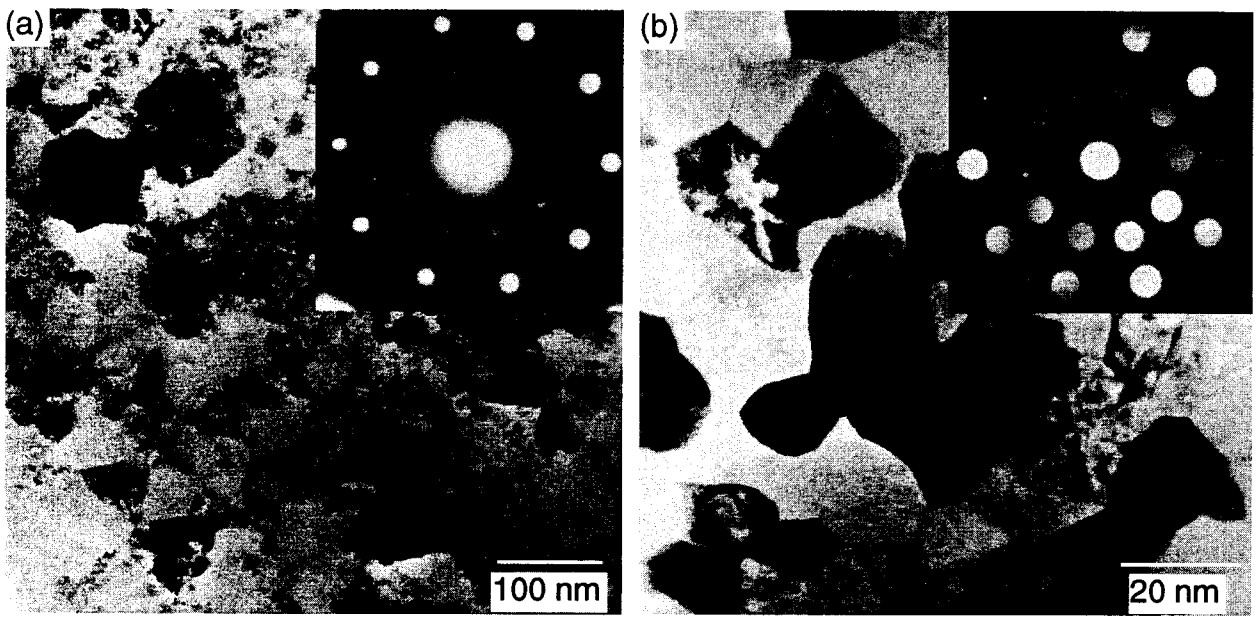

Fig. 2 TEM bright field images of (a) $Ti_{55}Zr_{20}Ni_{25}$ (inset is selected area electron diffraction from i-phase) and (b) $Zr_{55}Ti_{25}Ni_{20}$ alloys (inset is microdiffraction from i-phase) melt spun at 20 m/s.

is the same as that of the as melt spun alloy (Fig. 4), suggesting that the i-phase is stable in this alloy up to 873 K. The specimen at the other two wheel speeds exhibit one exotherm at around 840 K (Fig. 3(a) and Table 1). The enthalpy associated with the exotherm (Table 1) at both the wheel speeds is similar (~ -1.0 kJ/mol), suggesting that the amorphous phase transforms to the same phase at both wheel speeds. The XRD patterns of the alloy melt spun at 40 m/s and isochronally annealed specimen at 818 K indicate only amorphous halo, while that annealed at 873 K shows the presence of i-phase along with equilibrium phase mixture of Laves phase (TiZrNi), Ti_2Ni and α-(Ti, Zr) as evident from Fig. 5(a). The TEM study of the alloy melt spun at 40 m/s and that of isochronally annealed at 843 K (Fig. 6(a)) showed predominantly i-phase with a grain size of about 20–100 nm. Thus, the exotherm observed in the DSC trace of the Ti-rich alloy can be attributed, at least partly, to the nanoquasicrystallization of the amorphous phase.

The DSC traces of the Zr-rich alloy at different melt spun wheel velocities are depicted in Fig. 3(b). The alloy melt spun at 20 m/s has one exotherm at around 770 K, suggesting that the i-phase observed in the melt spun condition is not as stable as in the Ti-rich alloy and transforms to equilibrium phase mixture of TiZrNi, Zr_2Ni and α-(Zr, Ti). At the other melt spun wheel velocities, the alloy has two exotherms at around 640 and 760 K as shown in Fig. 3(b) and Table 1. The XRD (Fig. 5(b)) and TEM (Fig. 6(b)) studies of the alloy melt spun at 40 m/s and isochronally annealed at 708 K indicate the presence of i-phase, suggesting that the first exotherm in this alloy can be attributed to nanoquasicrystallization of the amorphous phase. Interestingly, the i-phase formed in the Zr-rich alloy isochronally annealed at about 70 K above the exothermic peak temperature (640 K) is much finer (~5–10 nm) than that formed in the Ti-rich alloy (20–

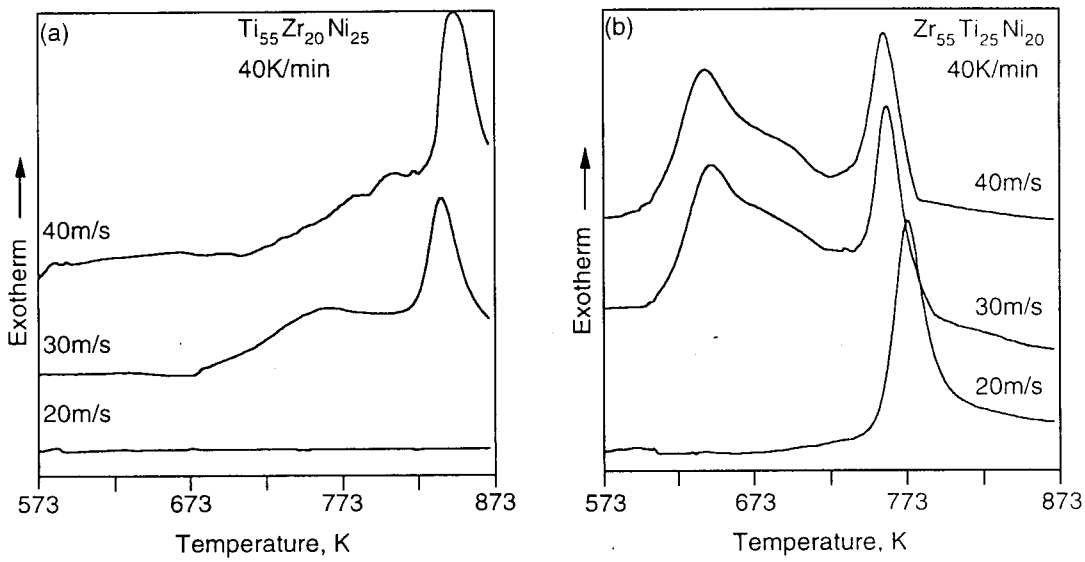

Fig. 3 DSC traces of (a) $Ti_{55}Zr_{20}Ni_{25}$ and (b) $Zr_{55}Ti_{25}Ni_{20}$ alloys as a function of melt spun wheel velocities at a heating rate of 40 K/min.

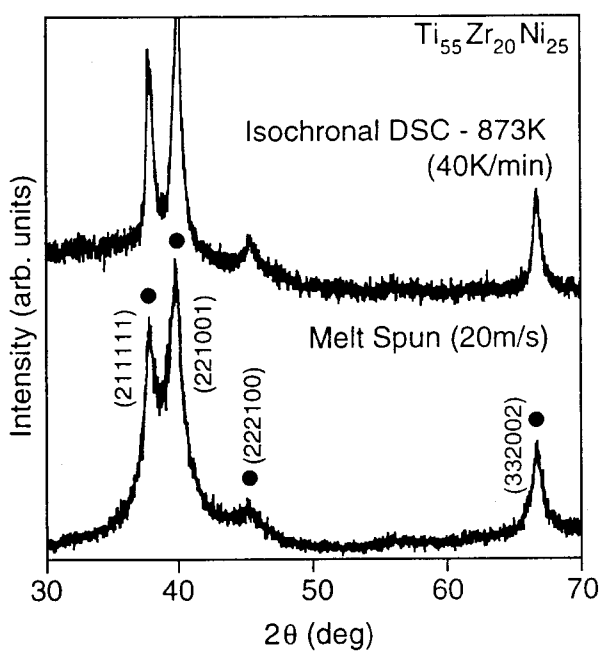

Fig. 4 XRD patterns of $Ti_{55}Zr_{20}Ni_{25}$ melt spun at 20 m/s and isochronally annealed in DSC at 873 K.

100 nm) that is annealed very close to the peak temperature (845 K). It can be recalled that the grain size of i-phase formed during melt spinning at 20 m/s is also finer in the Zr-rich alloy. This suggests that probably the nucleation rate of i-phase is higher in Zr-rich alloy and the growth rate is lower. The higher nucleation rate could be due to high negative enthalpy of mixing of Zr–Ni pair (−49 kJ/mol) when compared to Ti–Ni pair (−35 kJ/mol). This could probably increase the driving force for the formation of i-phase and thus lower the activation barrier for its nucleation in the Zr-rich alloy. The lower growth rate of i-phase in Zr-rich alloy could probably be attributed to the lower diffusion rates in this alloy due to larger atomic radius of Zr (0.159 nm) compared to Ti (0.145 nm). The i-phase formed in Zr-rich alloy during the first crystallization event transforms during the second crystallization stage

Table 1 Vicker's hardness and DSC results (heating rate: 40 K/min) of melt spun $Ti_{55}Zr_{20}Ni_{25}$ and $Zr_{55}Ti_{25}Ni_{20}$ alloys.

Alloy	Melt spun wheel Velocity (m/s)	VHN	Quasicrystallization peak Peak (K)	Quasicrystallization peak ΔH (kJ/mol)	Crystallization peak Peak (K)	Crystallization peak ΔH (kJ/mol)
$Ti_{55}Zr_{20}Ni_{25}$	20	755	—	—	—	—
	30	700	837	−1.2	—	—
	40	555	845	−1.0	—	—
$Zr_{55}Ti_{25}Ni_{20}$	20	610	—	—	773	−1.5
	30	375	644	−1.1	760	−1.2
	40	375	640	−2.0	757	−1.0

to TiZrNi, Zr_2Ni and α-(Zr, Ti) as shown in Fig. 5(b).

The Vicker's hardness measurements (Table 1) have shown that both the Ti-rich and Zr-rich alloys have significantly higher hardness in the nanoquasicrystalline state (755 and 610 VHN, respectively) compared to the amorphous state (555 and 375 VHN, respectively) in the melt spun condition. The hardness values of the Ti-rich and Zr-rich alloys increases further by nanoquasicrystallization of the amorphous phase to 810 and 620 VHN, respectively. Though, the Ti-rich alloy has higher hardness than the Zr-rich alloy, the extent of increase in hardness due to nanoquasicrystallization of the amorphous phase is higher in the latter (45 and 65%, respectively).

4. Conclusions

(1) I-phase is obtained in the nanocrystalline state in the $Ti_{55}Zr_{20}Ni_{25}$ and $Zr_{55}Ti_{25}Ni_{20}$ alloys melt spun at 20 m/s, while at higher melt spun wheel velocities (30 and 40 m/s), the alloys become amorphous.

(2) In both the alloys, nanoquasicrystallization of the amorphous phase is observed. While the i-phase is stable up to 873 K in Ti-rich alloy, it transforms to crystalline phases below this temperature in Zr-rich alloy.

(3) The i-phase formed both directly from the melt and the amorphous is much finer in Zr-rich alloy compared to Ti-

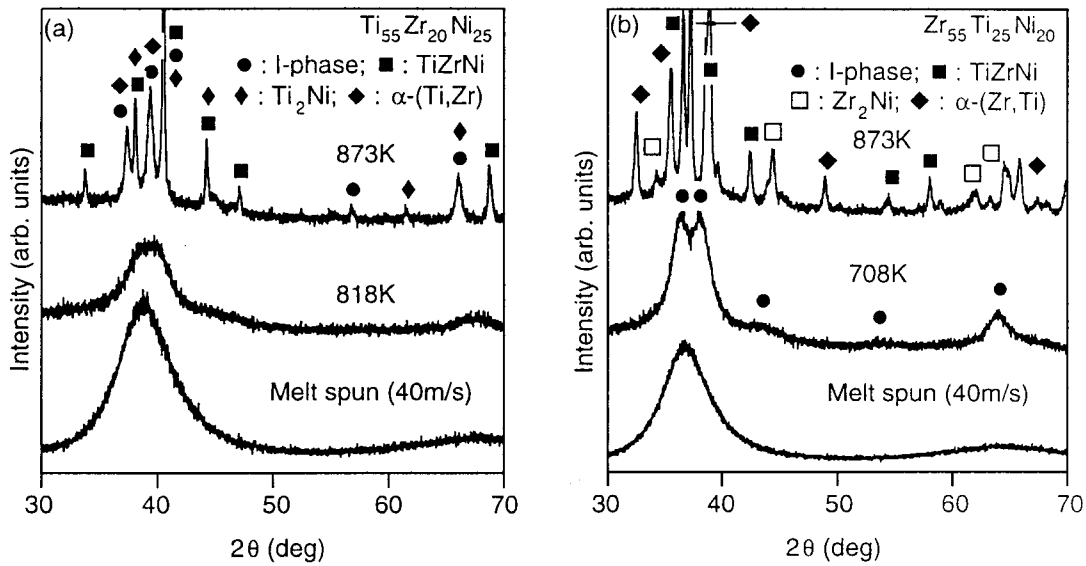

Fig. 5 XRD patterns of (a) $Ti_{55}Zr_{20}Ni_{25}$ and (b) $Zr_{55}Ti_{25}Ni_{20}$ alloys melt spun at 40 m/s and isochronally annealed at different temperatures.

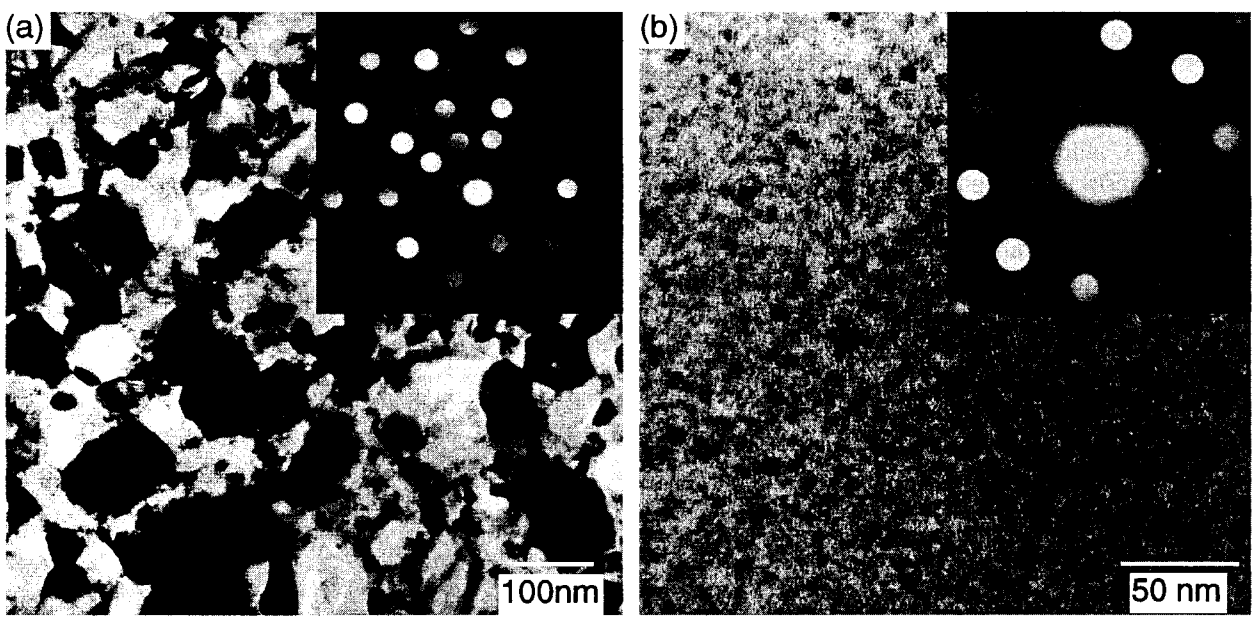

Fig. 6 TEM bright field images and microdiffraction patterns (insets) of (a) $Ti_{55}Zr_{20}Ni_{25}$ and (b) $Zr_{55}Ti_{25}Ni_{20}$ alloys melt spun at 40 m/s and subsequently isochronally annealed at 843 and 708 K, respectively.

rich alloy.

Acknowledgment

One of the authors (BSM) gratefully acknowledges the Japan Science and Technology Corporation for the provision of a STA fellowship.

REFERENCES

1) U. Köster, J. Meinhardt, S. Roos and H. Liebertz: Appl. Phys. Lett. **69** (1996) 179–181.
2) L. Q. Xing, J. Eckert, W. Löser and L. Schultz: Appl. Phys. Lett. **74** (1999) 664–666.
3) B. S. Murty, D. H. Ping, K. Hono and A. Inoue: Appl. Phys. Lett. **76** (2000) 55–57.
4) A. Inoue, T. Zhang, M. W. Chen, T. Sakurai, J. Saida and M. Matsushita: Appl. Phys. Lett. **76** (2000) 967–969.
5) J. Saida, M. Matsushita, C. Li and A. Inoue: Appl. Phys. Lett. **76** (2000) 3558–3560.
6) B. S. Murty, D. H. Ping, K. Hono and A. Inoue: Scripta Mater. **43** (2000) 103–107.
7) B. S. Murty, D. H. Ping and K. Hono: Appl. Phys. Lett. **77** (2000) 1102–1104.
8) J. Saida, M. Matsushita and A. Inoue: Appl. Phys. Lett. **77** (2000) 73–75.
9) B. S. Murty, D. H. Ping and K. Hono: unpublished work.
10) C. Li, J. Saida and A. Inoue: Scripta Mater. **42** (2000) 1077–1081.
11) V. V. Molokanov and V. N. Chebotnikov: J. Non-Crystal Solids **117/118** (1990) 789–792.
12) X. Zhang, R. M. Stroud, J. L. Libbert and K. F. Kelton: Philos. Mag. **70B** (1994) 927–950.
13) K. F. Kelton, W. J. Kim and R. M. Stroud: Appl. Phys. Lett. **70** (1997) 3230–3232.
14) V. Elser: Phys. Rev. B, **32** (1985) 4892–4898.